

## Electron Microscopic Study Using Formalin-fixed, Paraffin-embedded Material, with Special Reference to Observation of Microbial Organisms and Endocrine Granules

**Yutaka Tsutsumi**

*Division of Diagnostic Pathology, Haruhi Respiratory Medical Hospital, Kiyosu, Japan*

Received February 16, 2018; accepted March 8, 2018; published online April 19, 2018

In the diagnostic pathology practice, specimens for electron microscopy (EM) are not necessarily handled and fixed under the ideal condition. In the present article, the author describes ultrastructural study using formalin-fixed and/or paraffin-embedded material. The fine morphologic preservation is often acceptable, particularly when small cubes are dug out of paraffin blocks. Particulate structures such as neuroendocrine granules and microbes are consistently observed even using paraffin sections. Paraffin sections signalized with silver particles in Grimelius and Grocott stains or diaminobenzidine products in immunostaining and *in situ* hybridization are applicable to EM evaluation by using a pre-embedding sequence. The practical merit includes the targeted approach: highly accurate sampling from focal lesions can be achieved for EM analysis, after observing hematoxylin and eosin-stained or specific-signalized paraffin-sections. This allows us pathologists a convenient and practical way for identifying focally infected pathogens, as well as a retrospective ultrastructural analysis of rare lesions long kept as a form of paraffin blocks.

**Key words:** formalin-fixed paraffin-embedded material, electron microscopy, silver stain, neuroendocrine granules, pathogens

### I. Introduction

In the field of diagnostic pathology, electron microscopy (EM) is often requested to identify intracellular pathogens [10, 14, 20, 27, 47, 56] and neuroendocrine granules [18, 21, 26] in biopsy, surgical, autopsy and cytology specimens. It is particularly reproducible when the lesion is diffusely distributed in the specimen. When pathogens are localized in limited areas of tissues and organs, an orthodox EM approach may consume excessive time and effort. In order to evaluate the localized area in question ultrastructurally, a targeted approach is achieved in combination with

the observation at the light microscopic level. In the diagnostic pathology practice, EM study may be requested as a last resort by using formalin-fixed and/or paraffin-embedded material.

The author describes herein practical examples of EM study using formalin-fixed and/or paraffin-embedded human material. The target lesions are focused on neuroendocrine tumors and infections.

### II. Electron Microscopic Observation Using Formalin-fixed Material

In diagnostic pathology practice of EM study, glutaraldehyde fixation is not necessarily available, so that formalin-fixed material must be processed. Epon-embedded blocks should be prepared from formalin-fixed biopsy, surgical and autopsy samples [2, 7, 22, 45, 57, 62, 77, 78]. Even after long fixation in unbuffered acidic formalin solution, fine morphologic appearance is acceptable in many

Correspondence to: Yutaka Tsutsumi, M.D., Present address: Pathos Tsutsumi, 412 Palnes Zengo, 1735 Zene, Zengo-cho, Toyoake, Aichi 470-1151, Japan. E-mail: pathos223@kind.ocn.ne.jp

Invited article: A part of this article was presented as a workshop at the 58th Annual Meeting of the Japan Society of Histochemistry and Cytochemistry (Ehime 2017).

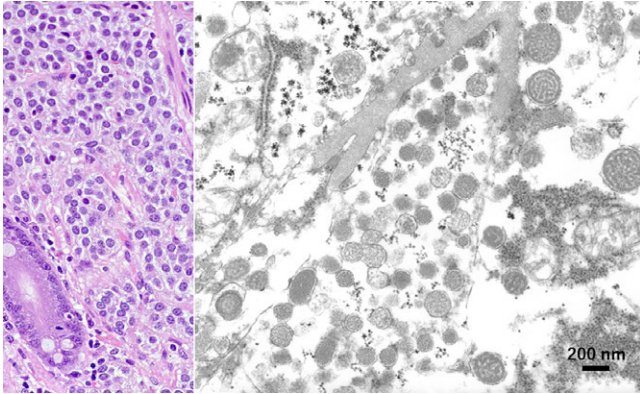


**Fig. 1.** Gastric carcinoid tumor surgically removed and fixed in unbuffered formalin (left: HE, right: EM). In the granular cytoplasm of the tumor cells, round and cored neuroendocrine-type granules, around 260 nm in diameter, are distributed. Cristae of mitochondria are retained. Bar = 200 nm.

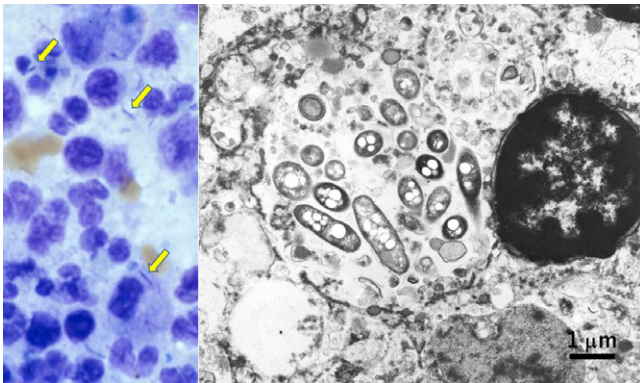


**Fig. 2.** Legionnaire's pneumonia fixed in unbuffered formalin (left: Giemsa stain of touch smear of the autopsy lung lesion, right: EM). In the cytoplasm of macrophages infiltrating in lobar pneumonia, rods are observed (arrows). Ultrastructurally, rod-shaped bacteria corresponding to *Legionella pneumophila* are phagocytized in lysosomes. Nuclear chromatin pattern is well preserved. Bar = 1 μm.

cases. In the author's experience, the most important point is to examine a well-fixed part of the specimen (namely, the cut surface of the material) for EM study. The quality of fine morphological preservation seems to be dependent on the initial fixation condition. Two representative examples are illustrated in Figures 1 and 2.

Large-sized gastric carcinoid tumor was surgically removed and soaked in unbuffered 10% formalin for weeks. EM study was performed using the formalin-fixed surgical material. Round cored granules, measuring 260 nm on average with a range from 150 to 380 nm, were clearly observed, and mitochondrial cristae were preserved, as shown in Figure 1.

An 88-year-old male died of acute respiratory failure four days after onset. Autopsy revealed lobar pneumonia in the right lower lobe, and Gram-negative rods corresponding to *Legionella pneumophila* were identified in phagosomes

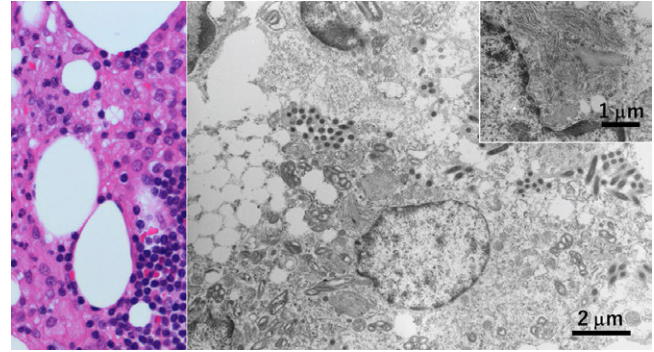


**Fig. 3.** Retroperitoneal lymph node of Whipple's disease fixed in formalin and embedded in paraffin (left: HE, right: EM). The biopsied nodal tissue is occupied by epithelioid/foamy histiocytes. Ultrastructurally, viable electron-dense rods corresponding to *Tropheryma whipplei* are clustered outside the cell, while the bacteria phagocytized by foamy macrophages are swollen and electron-lucent. Membranous residual bodies as a digested form of bacteria are multifocally observed in the lysosome (inset). Bar = 2 μm (inset: 1 μm).

of macrophages infiltrating in the alveolar space (Fig. 2). The diagnosis of legionnaire's pneumonia, common in the aged patient [9], was thus confirmed by EM study using routinely formalin-fixed autopsied lung tissue.

This approach is also applicable to non-neuroendocrine and non-infectious lesions. Fine morphology of tumor cells, including nuclear chromatin networks, mitochondria, endoplasmic reticula, intracellular filaments and junctional complexes, can successfully be evaluated using routinely formalin-fixed samples.

### III. Electron Microscopic Observation Using Formalin-fixed, Paraffin-embedded Blocks

When infective or neuroendocrine lesions are localized in a small area of the specimen, it is very difficult for us pathologists to detect the target structure at the ultrastructural level employing a conventional technique (random sampling). It has repeatedly been shown that the fine morphologic preservation is acceptable when small cubes are dug out of formalin-fixed, paraffin-embedded blocks [1, 8, 22, 33, 36, 45, 62, 70, 71, 73, 75, 76, 79]. After observing hematoxylin and eosin-stained paraffin-sections to aim at the target lesion, the corresponding paraffin block areas should be sampled as small cubes for EM study. Such targeted performance not only gives us a convenient and practical way for observing focally infected pathogens, but also allows us retrospective ultrastructural analysis of rare lesions long kept in paraffin blocks.

A representative example of EM analysis using formalin-fixed, paraffin-embedded blocks is demonstrated in Figure 3. A retroperitoneal lymph node was biopsied from a 70-year-old male clinically manifesting chronic diarrhea, weight loss and anemia. The node was occupied by clustered epithelioid macrophages. The possibility of

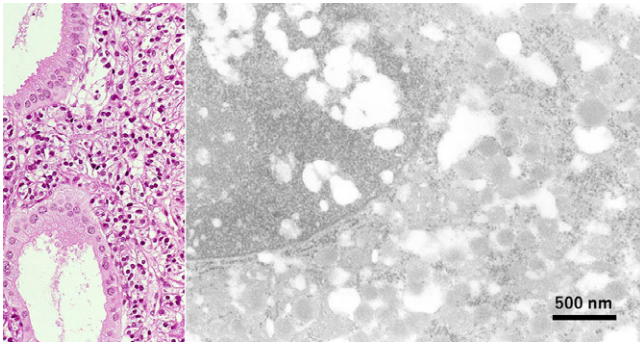


**Fig. 4.** Gallbladder carcinoid tumor in a formalin-fixed, paraffin-embedded section (left: HE, right: EM). A small polypoid pancreatic polypeptide-immunoreactive carcinoid tumor was totally embedded in paraffin. The tumor cells possess 200 nm-sized neuroendocrine granules with low electron density. The presence of a particulate structure such as neuroendocrine granules is well recognized ultrastructurally even after paraffin sectioning. Bar = 500 nm.

Whipple's disease was suspected both clinically and microscopically. No formalin-fixed nodal material remained, so that a paraffin block was used for EM study for confirming the diagnosis. Both inside and outside epithelioid macrophages, numerous rod-shaped bacteria corresponding to *Tropheryma whipplei* were identified [46]. Digested remnants of the bacteria were seen in lysosomes, characteristic features of Whipple's disease [16]. The fine morphological preservation is worthy of evaluation.

#### IV. Electron Microscopic Observation Using Paraffin Sections

In contrast to the use of paraffin blocks for EM analysis, the fine morphologic preservation is significantly poor when paraffin sections are processed for EM observation. A good number of trials of EM study using paraffin sections have been reported so far [1, 3, 22, 32, 42, 45, 53]. In the author's experience, particulate structures such as neuroendocrine granules and pathogenic microbes are worthy of observation even after paraffin sectioning. Ultrathin sections are prepared from the targeted area of paraffin sections after osmification and embedding in epoxy resin (Epon) blocks by the inverted beam capsule method (the pre-embedding sequence) [48, 50]. The targeted EM approach may contribute to diagnostic pathology.

A small polypoid carcinoid tumor was incidentally found in the stone-bearing gallbladder surgically removed from a 62-year-old female, and the lesion had totally been fixed in formalin and embedded in paraffin. The carcinoid tumor cells were consistently immunoreactive for pancreatic polypeptide. The presence of neuroendocrine granules was ultrastructurally evaluated using paraffin sections. Neuroendocrine-type cored granules, measuring 200 nm on average with an arrange of 130–290 nm, were identified in the cytoplasm of the tumor cells [63], as shown in Figure 4.

Bone marrow transplantation was performed in a 10-

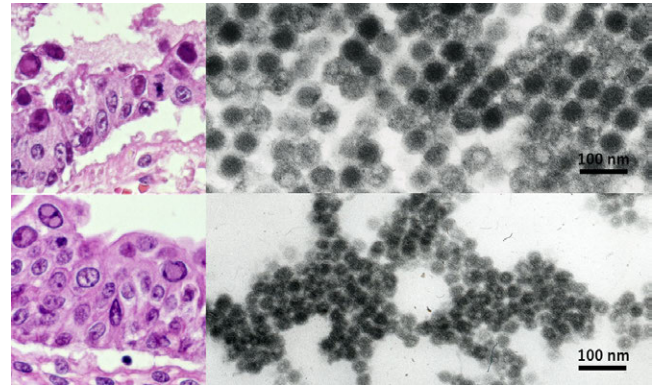


**Fig. 5.** Opportunistic dual infection of adenovirus and BK virus ultrastructurally identified in formalin-fixed, paraffin-embedded sections of autopsy material (left: HE, right: EM, top: small bowel mucosa, bottom: urinary bladder mucosa). Nuclear inclusion bodies of both smudge and cored types are indistinguishable at the light microscopic level. EM evaluation using paraffin sections contributed to identifying two different DNA viruses in the nuclei. Adenovirus larger than BK virus is hexagonal on cut surface and regularly arranged. Some adenoviral particles are vacant. Bars = 100 nm.

year-old boy suffering from acute lymphoblastic leukemia. Massive hematochezia occurred one week after transplantation and lasted for three months finally to kill the patient. At autopsy, viral nuclear inclusions of both smudge and cored types were discerned in the mucosa of the small intestine and urinary bladder. The targeted EM analysis was performed using paraffin sections. The nuclear inclusion bodies were caused by adenovirus in the small bowel and BK virus in the urinary bladder (Fig. 5). Adenovirus particles in the gut were geometrically arranged in the nucleus and were 70 nm in size and regular hexagonal in shape. Some particles were vacant without forming virions. BK virus particles in the bladder were smaller in size (40–55 nm) and randomly arranged in the nucleus. The light microscopic features of viral inclusions were indistinguishable each other, but opportunistic infection of two types of DNA viruses was confirmed by analyzing paraffin sections at the ultrastructural level [67, 68].

A pregnant 28-year-old female suffered from erythema infectiosum (slap-cheek) in the first trimester, and transplacental infection of human Parvovirus B19 caused hydrops fetalis and intrauterine fetal death [19]. A macerated fetus at the 25th gestational week, weighing 1,010 g, revealed marked anemia as grossly indicated by pale color of the 30 g liver. Nucleated red cells in capillary vessels in various organs often contained eosinophilic intranuclear inclusion bodies [28]. At first, the placenta was ultrastructurally sampled in a routine manner, but no viral inclusions were detected in randomly sampled Epon-embedded cubes. Therefore, formalin-fixed, paraffin-embedded sections of the placenta were evaluated for intranuclear viruses. As displayed in Figure 6, small viral particles, around 20 nm in diameter, were clustered in the nucleus of infected erythroblasts [67, 68].

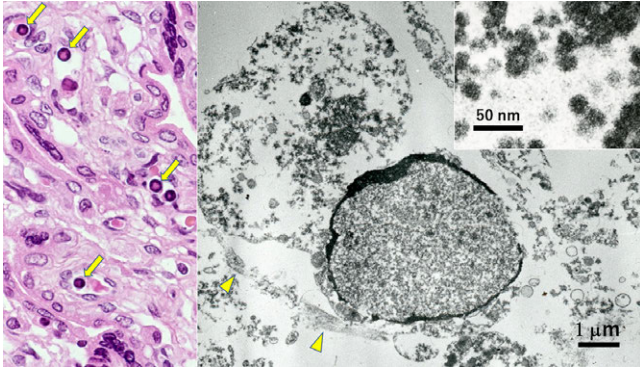


**Fig. 6.** Parvovirus B19-infected fetal erythroblasts EM-observed using formalin-fixed paraffin section of the placenta (left: HE, right: EM). Nucleated erythrocytes in capillary lumina often possess eosinophilic nuclear inclusions (arrows). Ultrastructurally, it is evident that the nucleus is filled with small-sized viruses, while fine morphologic preservation is very poor. Inset indicates 20 nm-sized viral particles. Arrowheads show endothelial lining of the capillary vessel wall. Bar = 1 µm (inset: 50 nm).

## V. Silver-impregnated Electron Microscopy Using Paraffin Sections

Silver impregnation-related staining techniques, such as Grimelius argyrophilic staining [24], Fontana-Masson argentaffin staining [39] and Grocott methenamine silver for fungi and related microbes [25, 58], are suitable for EM observation, because electron-dense silver grains are coarsely deposited at the specific site of reaction [1, 11, 12, 17, 45, 60]. Fontana-Masson's silver is known to be applicable to ultrathin sections with a post-embedding sequence to detect argentaffin endocrine granules and melanin-producing fungal bodies [38, 69]. The author exhibits herein representative pre-embedding application of Grimelius and Grocott staining to paraffin sections. Namely, the silver impregnated deparaffinized sections were processed for ultrathin sectioning after preparation of Epon-embedded blocks.

In Figure 7, argyrophilic (Grimelius-positive) neuroendocrine granules are demonstrated in paraffin sections of human fetal small bowel mucosa, pulmonary tumorlet (neuroendocrine cell hyperplasia associated with a fibrotic lung lesion [64]) and argyrophilic diffuse-type scirrhous gastric carcinoma [61]. Although fine morphologic preservation was poor, the presence of argyrophilic granules was clearly demonstrated in each case. The targeted observation was quite useful to identify neuroendocrine granules in pulmonary tumorlet presenting a grossly invisible minute lesion. Of note is that the peripheral halo of the granule was argyrophilic [5, 6, 69]. Small-sized neuroendocrine granules in pulmonary tumorlet especially exhibited peripherally oriented argyrophilic silver grain deposition. The halo is known to be the site of localization of chromogranin A, a

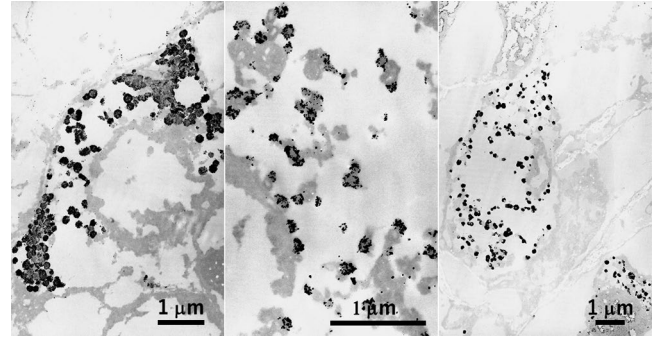


**Fig. 7.** Grimelius silver reaction at the EM level in human fetal small bowel mucosa (left), pulmonary tumorlet (center) and argyrophilic scirrhous gastric cancer (right) in paraffin sections. Argyrophilic reactions are focused on the cored granules in the respective neuroendocrine-type cells. Silver grains are clustered in the peripheral halo area, and this is particularly evident in small-sized granules in pulmonary tumorlet. Background staining is minimal. Bars = 1 µm.

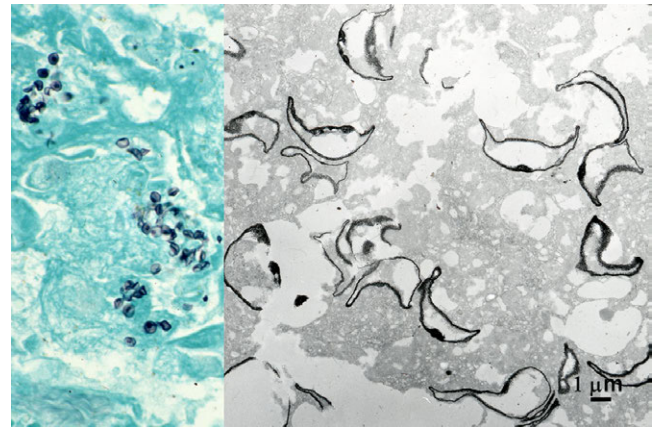


**Fig. 8.** Grocott stain in pneumocystosis in paraffin sections of lung biopsy at the light and electron microscopic levels. The cyst wall of *Pneumocystis jirovecii* is densely silver-impregnated. Alveolar space is filled with the black-signal, crescent-shaped pathogen. Dot-like signals as focal thickening of the cell wall are observed at both light and electron microscopic levels. Bar = 1 µm.

common carrier protein of the neuroendocrine granules [72].

Pneumocystosis is often encountered as opportunistic lung infection in acquired immunodeficiency syndrome (AIDS) [44]. Cysts of *Pneumocystis jirovecii* are demonstrated with Grocott methenamine silver. The Grocott-stained paraffin section sampled by transbronchial lung biopsy from an AIDS patient was embedded by the inverted beam capsule method in Epon blocks, and ultrathin sections were observed on an electron microscope. The cyst wall and internal dot-like structure were clearly labeled by silver grains [67] (Fig. 8). The crescent-shaped cysts measured 5–8 µm. Background staining was minimal.

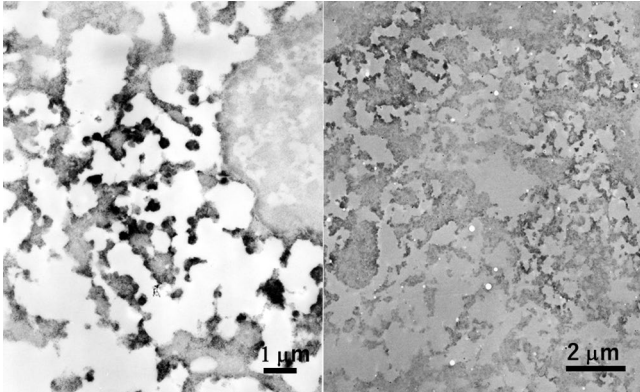


**Fig. 9.** Ectopic insulinoma of the duodenum (left) and calcitonin-positive large cell neuroendocrine carcinoma of the lung (right) immunostained in paraffin sections and processed for EM observation. The cytoplasm is abundant in round-shaped granules immunoreactive for insulin or calcitonin and measuring around 200 nm. The margin of the positively signaled granules is obscure in both cases. The preservation of background fine morphology is poor. Bars = 1  $\mu\text{m}$  (left) and 2  $\mu\text{m}$  (right).

## VI. Immunoelectron Microscopy and Ultrastructural *In Situ* Hybridization Using Paraffin Sections

Neuroendocrine granules and microbes are clearly and consistently demonstrated in paraffin sections by immunostaining using specific antibodies and/or *in situ* hybridization (ISH) using specific probes. The routinely prepared and stained paraffin sections are further processed for EM observation [13]. In infectious lesions, in particular, the pathogens are often distributed in localized small areas, so that the targeted EM observation is reasonably needed [66]. First, the target molecules were visualized with immunostaining or ISH as brown diaminobenzidine deposits. After observation and photographing under a light microscope, the cover slip was removed in xylene and the section is subsequently osmified. The area with positive signals was targeted to prepare Epon-embedded ultrathin sections by the inverted beam capsule method.

The author's group further identified neutrophil extracellular traps (NETs), formed in infectious lesions, by employing immunocytochemistry at the light and electron microscopic levels [54, 55, 59]. NETs, a fine filamentous network deriving from dead neutrophils in inflammatory foci, consist of anti-bacterial components of the granules deposited on degraded chromatin thread [4]. The main target of our investigation was formalin-fixed, paraffin-embedded autopsy material of legionnaire's pneumonia. Lactoferrin was useful as a marker of NETs.

Neuroendocrine granules with specific immunoreactive signals were ultrastructurally visualized in paraffin sections of insulinoma and calcitonin-positive large cell neuroendocrine carcinoma of the lung (Fig. 9). Insulinoma was ectopically seen in the duodenum [74]. Osmified

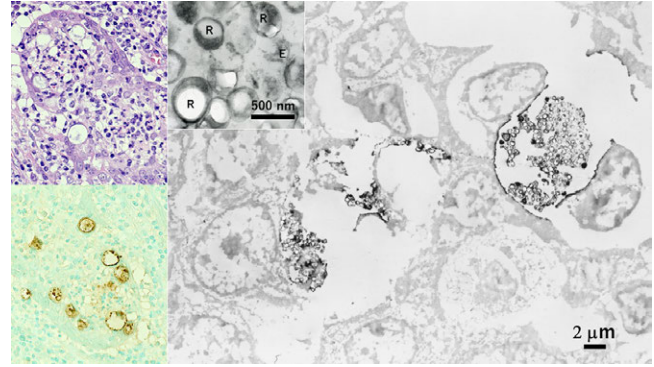


**Fig. 10.** Chlamydial epididymitis immunostained in paraffin sections and processed for EM observation (left top: HE, left bottom and right: immunostaining for chlamydial antigen). Labeled signals are clustered in the dotted inclusion bodies formed in the cytoplasm of epididymal ductal cells. At the EM level, the cell wall of the pathogens shows distinct positive signals. At high magnification, large-sized proliferative form (reticulate body: R) and smaller infective form (elementary body: E) are recognized (inset). Bars = 2  $\mu\text{m}$  (inset: 500 nm).

diaminobenzidine signals of insulin and calcitonin were aggregated on the 200 nm-sized cored granules clustered in the cytoplasm of tumor cells, though diffusion of reaction products was inevitable.

*Chlamydia trachomatis* causes sexually transmitted disease in the uterine cervix, oviduct, male urethra and epididymis [37]. A 28-year-old male complained of scrotal swelling, and surgical excision was performed under the clinical diagnosis of epididymal tumor. Histologically, vacuolar cytoplasmic inclusions were seen in the epididymal ductal cells surrounded by chronic active inflammation. Immunohistochemical positivity of *C. trachomatis* antigen (detected by a monoclonal antibody, clone B104.1) in the inclusions confirmed the diagnosis [30, 66]. The immunostained paraffin section was osmified and embedded in Epon blocks to observe ultrastructural appearance. The cell wall of chlamydial particles showed distinct positive signals. At high magnification, large-sized proliferative form (reticulate body) and smaller infective form (elementary body) were recognized (Fig. 10).

Similarly, a variety of intracellular bacillary microbes in paraffin sections were proven ultrastructurally [67, 68]. *Escherichia coli* antigens were detected in foamy macrophages in xanthogranulomatous cholecystitis [43] and in purulent epididymitis [29, 66]. *Helicobacter pylori* antigens were localized in gastric xanthoma cells [31]. Bacillus Calmet Guerin (BCG) antigens were visualized in "striated histiocytes" infected by *Mycobacterium avium intracellulare* [35] and in "globi" in lepromatous leprosy caused by *Mycobacterium leprae* [40]. Positively stained loci were targeted for EM study. Macrophages in the respective infectious lesions contained positively signaled rod-shaped bacteria (Fig. 11).

Cytomegalovirus (CMV) seen in the autopsied lung

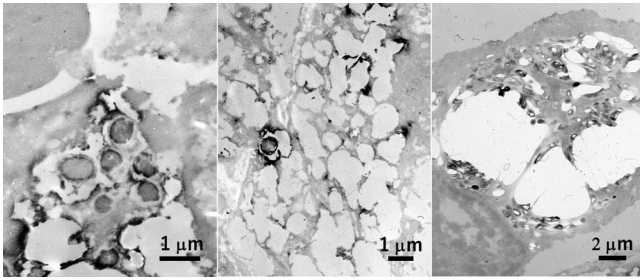


**Fig. 11.** Rods ultrastructurally visualized in the cytoplasm of macrophages in xanthogranulomatous cholecystitis (left), gastric xanthoma (center) and nodal non-tuberculous mycobacteriosis in AIDS (right). Immunostaining using commercial antisera against *Escherichia coli* (left), *Helicobacter pylori* (center) and BCG (right) was performed in paraffin sections, respectively. Of note is that the bacilli are packed in the cytoplasm of so-called “striated histiocyte” in the latter lesion. Bars = 1 µm (left and center) and 2 µm (right).

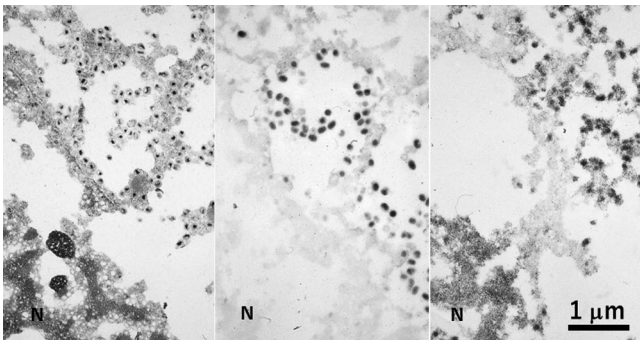


**Fig. 12.** A CMV-infected pneumocyte in autopsied and paraffin-embedded lung tissue consecutively observed by conventional EM (left), immunostaining (center) and ISH (right). In spite of poor morphologic preservation, enveloped cored viral particles are clearly seen in the cytoplasm, while the nuclei are packed with virions without envelope. Immunoelectron microscopy using an antiserum against envelope protein discloses enveloped particles in the cytoplasm, while ISH detects the viral genome in both the cytoplasmic viral particles and envelope-less virions clustered in the nuclear matrix. N = nucleus. Bar = 1 µm.

was specifically demonstrated in paraffin sections with immunostaining and ISH, and subsequently visualized at the ultrastructural level (Fig. 12). CMV antiserum available from Polysciences, Inc (Warrington, PA, USA) detecting envelope antigens labeled cytoplasmic viral inclusions without signals in nuclear inclusions. At the ultrastructural level, the viral particles in the cytoplasm were sharply reacted by both techniques [34]. Viral DNA was demonstrated in clustered virions without envelopes in the nuclear matrix of the infected and enlarged pneumocyte [66, 67].

Severe fever with thrombocytopenia syndrome (SFTS), caused by SFTS virus infection mediated through tick bite, is endemic in the western part of Japan [52]. Lymph nodes, spleen and gastrointestinal tract are known to be the main target organs. The nodal lesion reveals necrotizing lymphadenitis-like change with active apoptosis and hemophagocytosis, representing hypercytokinemia

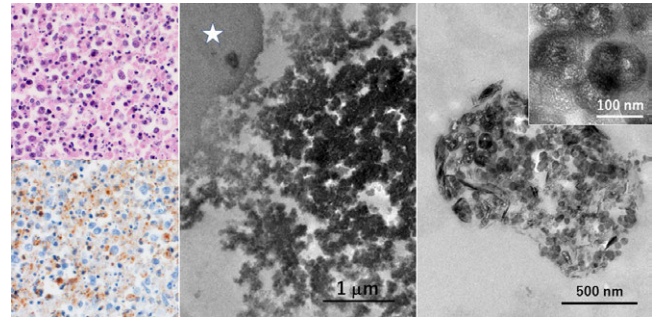


**Fig. 13.** Ultrastructural detection of viral particles in the lymph node of SFTS in formalin-fixed, paraffin-embedded sections (left top: HE, left bottom and center: immunostaining using a monoclonal antibody clone 1C3, right: ISH by the AT-tailing method using biotinylated antisense cocktail probes). Necrotizing lymphadenitis-like features are discerned in the enlarged node. Viruses are distributed in the cytoplasm of hemophagocytic macrophages. At the ultrastructural level, the labeled viral particles are round in shape and around 100 nm in size. Asterisk indicates a phagocytized erythrocyte. TACAS™ slides allowed both the prevention of slide detachment during heating pretreatment and transfer of the stained paraffin section to the Epon block. Bars = 1 µm (center), 500 nm (right) and 100 nm (inset).

[51]. SFTS virus was detected in paraffin sections of the lymph node of a lethal autopsy case (an 86-year-old female) by immunostaining and ISH, and dot-like positive signals were distributed in the cytoplasm of hemophagocytic macrophages. The AT-tailing method [49] was employed for detecting the viral genome. TACAS™ (Thinlayer Advanced Cytology Assay System) slides available from Medical Biological Laboratory, Nagoya, Japan, were useful for this purpose. The TACAS slides uniquely allowed two reciprocal functions: namely, during staining requiring heating pretreatment they must prevent detaching off sections, but after staining the sections can be transferred to Epon blocks [41]. At the ultrastructural level, the electron-dense diaminobenzidine products were clustered on round-shaped viral particles, around 100 nm in diameter, visualized by both techniques (Fig. 13).

## VII. Immunoelectron Microscopy and Ultrastructural *In Situ* Hybridization Using Ethanol-fixed Cytology Specimen

Immunoelectron microscopic demonstration of *Chlamydia trachomatis* particles in ethanol-fixed cervical cytology specimen was already reported [29]. Chlamydial antigen-positive signals in a metaplastic cell seen in a single cytology slide was successfully visualized at the ultrastructural level. The result was comparable with that obtained in the paraffin section, as illustrated in Figure 10.

The genome of human papillomavirus (HPV), causing a variety of sexually transmitted genital disorders [15], was demonstrated by ISH using multivalent biotinylated probes in the koilocytic nucleus of mild dysplasia in a cervical smear preparation. The positive intranuclear signals were subsequently observed at the ultrastructural level, as seen in

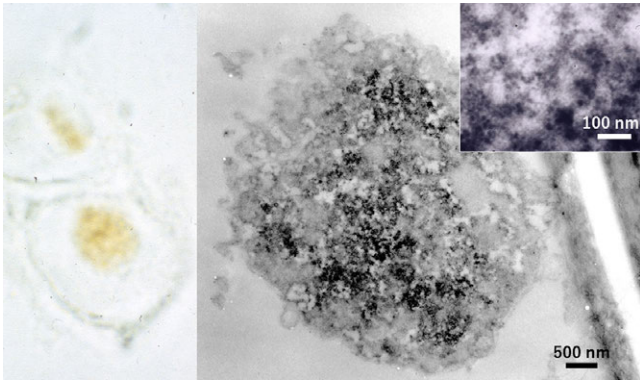


**Fig. 14.** HPV genome in an alcohol-fixed cytology specimen of mild dysplasia of the uterine cervix, visualized by ISH using polyvalent probes for HPV at the light microscopic (left) and electron microscopic (right) levels. The nuclear matrix of the koilocyte shows fine granular positivity. High-powered view (inset) reveals 20 nm-sized positive signals, representing episomed viral genome. Bar = 500 nm (inset: 100 nm).

Figure 14. The size of labeled intranuclear particles was around 20 nm, much smaller than the viral particle of HPV (around 50 nm in diameter) [67]. The represents episomes (naked viral DNA without forming viral particles [23]) in the dysplastic cell. Paraffin sections were also applicable to visualize the intranuclear form of HPV in verruca vulgaris of the skin, condyloma acuminatum of the penis and severe dysplasia of the uterine cervix, as reported previously [65, 66]. Immunostaining using antiserum against HPV capsid antigens was applied to the verrucous lesion, ISH with probes of HPV type 6/11 for the condyloma, and ISH with probes of HPV 16/18 for the dysplastic lesion. The nuclei contained viral particles 50 nm in size in verruca, 20 nm-sized episome forms in condyloma, and chromosome-integrated focal dotted signals in severe dysplasia.

### VIII. Conclusions

In diagnostic pathology, needs of EM study are undoubtedly decreasing along with remarkable progresses in molecular pathology. EM evaluation is now often outsourced to laboratory services even in university or large-sized hospitals in Japan. Despite the shrinking course of history of EM medical service, the author would like to emphasize the importance and availability of EM detection of infectious agents. The convenience of utilizing routinely prepared (formalin-fixed, paraffin-embedded) material for EM study should be re-evaluated. The approach described here will contribute not only to making an appropriate pathology diagnosis but also to understanding the disease process and pathogenesis.

### IX. Conflicts of Interest

There is no conflicts of interest in the present study.

### X. Acknowledgments

The technical assistance by Takanori Onouchi, Ph.D., Joint Research Laboratory, Fujita Health University, Toyoake, Japan, is cordially acknowledged. The author sincerely thanks many colleague technologists in the Division of Diagnostic Pathology, Tokai University Hospitals, Isehara, Japan, who gave the author continuous support and excellent skills. The present review was presented in the workshop session entitled “New application of electron microscopy” at the 58th Annual Meeting of the Japanese Society of Histochemistry and Cytochemistry in To-on, Ehime, in September 24th, 2017.

### XI. References

- Asato, T., Munakata, S., Ichiki, Y., Izumiya, N., Iwasaka, S., Sakamoto, M., Shiozawa, Y., Tachibana, T., Hirohata, Y., Morishita, Y. and Yoshida, M. (1998) Re-embedding of formalin-fixed and paraffin-embedded specimens with Epon. *J. Electron Microsc.* 33; 54–56 (in Japanese with English abstract).
- Ashworth, C. T. and Stembridge, V. A. (1964) Utility of formalin-fixed surgical and autopsy specimens for electron microscopy. *Am. J. Clin. Pathol.* 42; 466–480.
- Bretschneider, A., Burns, W. and Morrison, A. (1981) “Pop-off” technic. The ultrastructure of paraffin-embedded sections. *Am. J. Clin. Pathol.* 76; 450–453.
- Brinkmann, V., Reichard, U., Goosmann, C., Fauler, B., Uhlemann, Y., Weiss, D. S., Weinrauch, Y. and Zychlinsky, A. (2004) Neutrophil extracellular traps kill bacteria. *Science* 303; 1532–1535.
- Bussolati, G., Capella, C., Vassallo, G. and Solcia, E. (1971) Histochemical and ultrastructural studies on pancreatic A cells. Evidence for glucagon and non-glucagon components of the  $\alpha$  granule. *Diabetologia* 7; 181–188.
- Capella, C. and Solcia, E. (1972) The endocrine cells of the pig gastrointestinal mucosa and pancreas. *Arch. Histol. Jpn.* 35; 1–29.
- Carson, F. L., Martin, J. H. and Lynn, J. A. (1972) Formalin fixation for electron microscopy: a re-evaluation. *Am. J. Clin. Pathol.* 59; 365–373.
- Cheville, N. F. and Stasko, J. (2014) Techniques in electron microscopy of animal tissue. *Vet. Pathol.* 51; 28–41.
- Cunha, B. A., Burillo, A. and Bouza, E. (2016) Legionnaires’ disease. *Lancet* 387; 376–385.
- Curry, A., Appleton, H. and Dowsett, B. (2006) Application of transmission electron microscopy to the clinical study of viral and bacterial infections: present and future. *Micron* 37; 91–106.
- Dawson, P. A. and Filipe, M. I. (1976) An ultrastructural application of silver methenamine to the study of mucin changes in the colonic mucosa adjacent to and remote from carcinoma. *Histochem. J.* 8; 143–158.
- de Martino, C. and Zamboni, L. (1967) Silver methenamine stain for electron microscopy. *J. Ultrastruct. Res.* 19; 273–282.
- Dingemans, K. P. and Ramkema, M. (2001) Immunoelectron microscopy on material retrieved from paraffin: accurate sampling on the basis of stained paraffin sections. *Ultrastruct. Pathol.* 25; 201–206.
- Doane, F. W. and Anderson, N. (1987) *Electron Microscopy in Diagnostic Virology: A Practical Guide and Atlas*. Cambridge University Press, Cambridge, UK.
- Doorbar, J., Egawa, N., Griffin, H., Kranjec, C. and Murakami, I.

- (2015) Human papillomavirus molecular biology and disease association. *Med. Virol.* 25(Suppl. S1); 2–23.
16. Ectors, N. L., Geboes, K. J., de Vos, R. M., Heidbuchel, H. P., Rutgeerts, P. J., Desmet, V. J. and Vantrappen, G. R. (1994) Whipple's disease: a histological, immunocytochemical, and electron microscopic study of the small intestinal epithelium. *J. Pathol.* 172; 73–79.
  17. Franzen, A. J., Cunha, M. M., Miranda, K., Hentschel, J., Plattner, H., da Silva, M. B., Salgado, C. G., de Souza, W. and Rozental, S. (2008) Ultrastructural characterization of melanosomes of the human pathogenic fungus *Fonsecaea pedrosoi*. *J. Struct. Biol.* 162; 75–84.
  18. Ghadially, F. N. (1985) Diagnostic Electron Microscopy of Tumours (2nd Ed). Butterworth-Heinemann Elsevier, Oxford, UK.
  19. Giorgio, E., de Oronzo, M. A., Iozza, I., di Natale, A., Cianci, S., Garofalo, G., Giacobbe, A. N. and Politi, S. (2010) Parvovirus B19 during pregnancy: a review. *J. Prenat. Med.* 4; 63–66.
  20. Goldsmith, C. S. and Miller, S. E. (2009) Modern uses of electron microscopy for detection of viruses. *Clin. Microbiol. Rev.* 22; 552–563.
  21. Graham, A. R., Payne, C. M., Nagle, R. B. and Angel, E. (1987) The role of immunohistochemistry, electron microscopy and ultrastructural cytochemistry in the diagnosis of mixed carcinoma-neuroendocrine neoplasms. *Pathol. Res. Pract.* 182; 23–33.
  22. Graham, L. and Orenstein, J. M. (2007) Processing tissue and cells for transmission electron microscopy in diagnostic pathology and research. *Nat. Protoc.* 2; 2439–2450.
  23. Greber, U. F. and Fassati, A. (2003) Nuclear import of viral DNA genomes. *Traffic* 4; 136–143.
  24. Grimelius, L. (1968) A silver nitrate stain for A2 cells of human pancreatic islets. *Acta Soc. Med. Ups.* 73; 243–270.
  25. Grocott, R. G. (1955) A stain for fungi in tissue sections and smears using Gomori's methenamine-silver nitrate technic. *Am. J. Pathol.* 25; 975–979.
  26. Hammond, E. H., Yowell, R. L. and Flinner, R. L. (1998) Neuroendocrine carcinomas: role of immunocytochemistry and electron microscopy. *Hum. Pathol.* 29; 1367–1371.
  27. Hazelton, P. R. and Gelderblom, H. R. (2003) Electron microscopy for rapid diagnosis of emerging infectious agents. *Emerg. Infect. Dis.* 9; 294–303.
  28. Hirazono, K., Shinozuka, T., Fujii, A., Hori, S., Itoh, H., Kawai, K., Satoh, S. and Osamura, R. Y. (1992) A case of human parvovirus B19 infection associated with hydrops fetalis. *Nihon Rinsho Saibo Gakkai Zasshi* 31; 1069–1074 (in Japanese with English abstract).
  29. Hori, S., Itoh, H., Tsutsumi, Y. and Osamura, R. Y. (1995) Immunoelectron microscopic detection of chlamydial antigens in Papanicolaou-stained routine vaginal smears. *Acta Cytol.* 39; 835–837.
  30. Hori, S. and Tsutsumi, Y. (1995) Histologic differentiation between chlamydial and bacterial epididymitis: nondestructive and proliferative versus destructive and abscess-forming. Immunohistochemical and clinicopathological findings. *Hum. Pathol.* 26; 402–407.
  31. Hori, S. and Tsutsumi, Y. (1996) *Helicobacter pylori* infection in gastric xanthomas: immunohistochemical analysis of 145 lesions. *Pathol. Int.* 46; 589–593.
  32. Hultquist, G. T. and Karlsson, U. (1972) Use of formalin-fixed, paraffin-embedded biopsy or autopsy material for electron microscopy. *Pathol. Eur.* 7; 97–101.
  33. Johannessen, J. V. (1977) Use of paraffin material for electron microscopy. *Pathol. Annu.* 12; 189–224.
  34. Kawai, K., Hori, S., Yamazaki, H. and Osamura, R. Y. (1989) Detection of cytomegalovirus in paraffin sections by *in situ* hybridization. *Byori Gijutsu* 39; 13–18 (in Japanese).
  35. Klatt, E. C., Jensen, D. F. and Meyer, P. R. (1987) Pathology of *Mycobacterium avium-intracellulare* infection in acquired immunodeficiency syndrome. *Hum. Pathol.* 18; 709–714.
  36. Lehner, T., Nunn, R. E. and Pearse, A. G. E. (1966) Electron microscopy of paraffin-embedded material in amyloidosis. *J. Pathol.* 91; 297–300.
  37. Manavi, K. (2006) A review on infection with *Chlamydia trachomatis*. *Best Pract. Res. Clin. Obstet. Gynaecol.* 20; 941–951.
  38. Marinozzi, V. (1961) Silver impregnation of ultrathin sections for electron microscopy. *J. Biophys. Biochem. Cytol.* 9; 121–133.
  39. Masson, P. (1928) Carcinoids (argentaffin tumors) and nerve hyperplasia of appendicular mucosa. *Am. J. Pathol.* 4; 181–211.
  40. Massone, C., Belachew, W. A. and Schettini, A. (2015) Histopathology of the lepromatous skin biopsy. *Clin. Dermatol.* 33; 38–45.
  41. Matsui, T., Onouchi, T., Shioyama, K., Mizutani, Y., Inada, K., Yu, F., Hayasaka, D., Morita, K., Ogawa, H., Mahara, F. and Tsutsumi, Y. (2015) Coated glass slides TACAS are applicable to heat-assisted immunostaining and *in situ* hybridization at the electron microscopy level. *Acta Histochem. Cytochem.* 48; 153–157.
  42. Mitomo, Y. and Miyamoto, H. (1972) Electron microscopic observation of routinely paraffin-embedded sections for pathological study. Dual observation of light and electron microscopy. *Igaku-no-Ayumi* 83; 593–596 (in Japanese).
  43. Mori, M., Watanabe, M., Sakuma, M. and Tsutsumi, Y. (1999) Infectious etiology of xanthogranulomatous cholecystitis: immunohistochemical identification of bacterial antigens in the xanthogranulomatous lesions. *Pathol. Int.* 49; 849–852.
  44. Morris, A. and Norris, K. A. (2012) Colonization by *Pneumocystis jirovecii* and its role in disease. *Clin. Microbiol. Rev.* 25; 297–317.
  45. Munakata, S., Park, P., Umamoto, M., Matsunaga, R., Sakuma, A., Koyama, Y., Ohno, T., Shimada, K. and Nagao, K. (1993) "Re-embedding electron microscopy". *J. Electron Microsc. Technol. Med. Biol.* 7; 84–90 (in Japanese).
  46. Nagasue, T., Kurahara, K., Yaita, H., Tanaka, T., Oshiro, Y., Kuno, N., Harada, A., Kameda, M., Iwasaki, K. and Tsutsumi, Y. (2016) Whipple's disease diagnosed using electron microscopy and polymerase chain reaction. *Nihon Shokakibyō Gakkai Zasshi* 113; 1894–1900 (in Japanese with English abstract).
  47. Nagata, N. and Sata, T. (2013) Detection of pathogens using electron microscopy. *Mod. Media* 59; 34–40 (in Japanese).
  48. Nagura, H., Nakane, P. K. and Brown, W. R. (1979) Translocation of dimetric IgA through neoplastic colon cells *in vitro*. *J. Immunol.* 123; 2359–2368.
  49. Nakajima, N., Ionescu, P., Sato, Y., Hashimoto, M., Kuroita, T., Takahashi, H., Yoshikura, H. and Sata, T. (2003) *In situ* hybridization AT-tailing with catalyzed signal amplification for sensitive and specific *in situ* detection of human immunodeficiency virus-1 mRNA in formalin-fixed and paraffin-embedded tissues. *Am. J. Pathol.* 162; 381–389.
  50. Nakane, P. K. (1968) Simultaneous localization of multiple tissue antigens using the peroxidase-labeled antibody method: a study on pituitary glands of the rat. *J. Histochem. Cytochem.* 16; 557–560.
  51. Nakano, A., Ogawa, H., Nakanishi, Y., Fujita, H., Mahara, F., Shioyama, K., Tsutsumi, Y. and Takeichi, T. (2017) Hemophagocytic lymphohistiocytosis in a fatal case of severe fever with thrombocytopenia syndrome. *Intern. Med.* 56; 1597–1602.
  52. National Institute of Infectious Diseases (2014) Severe Fever with Thrombocytopenia Syndrome (SFTS) Medical Care Hand-

- book (English Version) SFTS Handbook 2014 April\_engl(1).pdf
53. Ngai, H. K., Chan, K. W., Or, S. B. and Yau, W. L. (1985) A rapid method for reprocessing paraffin sections for diagnostic electron microscopy. *J. Pathol.* 145; 59–62.
  54. Onouchi, T., Shiogama, K., Matsui, T., Mizutani, Y., Sakurai, K., Inada, K. and Tsutsumi, Y. (2016) Visualization of neutrophil extracellular traps and fibrin meshwork in human fibrinopurulent inflammatory lesions. II. Ultrastructural study. *Acta Histochem. Cytochem.* 49; 117–123.
  55. Onouchi, T., Shiogama, K., Mizutani, Y., Takaki, T. and Tsutsumi, Y. (2016) Visualization of neutrophil extracellular traps and fibrin meshwork in human fibrinopurulent inflammatory lesions. III. Correlative light and electron microscopic study. *Acta Histochem. Cytochem.* 49; 141–147.
  56. Roingeard, P. (2008) Viral detection by electron microscopy: past, present and future. *Biol. Cell* 100; 491–501.
  57. Shindo, N., Okada, M., Oami, H. and Yamamoto, E. (1982) An electron microscopic observation on the tissue fixed with a routine buffered formalin fixative. I. *Iryo* 36; 403–453 (in Japanese with English abstract).
  58. Shiogama, K., Kitazawa, K., Mizutani, Y., Onouchi, T., Inada, K. and Tsutsumi, Y. (2015) New Grocott stain without using chromic acid. *Acta Histochem. Cytochem.* 48; 9–14.
  59. Shiogama, K., Onouchi, T., Mizutani, Y., Sakurai, K., Inada, K. and Tsutsumi, Y. (2016) Visualization of neutrophil extracellular traps and fibrin meshwork in human fibrinopurulent inflammatory lesions. I. Light microscopic study. *Acta Histochem. Cytochem.* 49; 109–116.
  60. Soranzo, L. and Roland, J. (1987) Application of Grimelius argyrophil staining to the study of tumour ultrastructure: I. Effects of fixatives. *Acta Histochem.* 81; 199–221.
  61. Tahara, E., Ito, H., Nakagami, K., Shimamoto, F., Yamamoto, M. and Sumii, K. (1982) Scirrhus argyrophil cell carcinoma of the stomach with multiple production of polypeptide hormones, amine, CEA, lysozyme, and HCG. *Cancer* 49; 1904–1915.
  62. Takaki, T. (2008) Limitations in application of formalin-fixed and/or paraffin-embedded tissue to electron microscopy. *Byori Gijutsu* 71; 28–34 (in Japanese).
  63. Tanaka, K., Iida, Y. and Tsutsumi, Y. (1992) Pancreatic polypeptide-immunoreactive gallbladder carcinoid tumor. *Acta Pathol. Jpn.* 42; 115–118.
  64. Tsutsumi, Y., Osamura, R. Y., Watanabe, K. and Yanaiharu, N. (1987) Immunohistochemical studies on gastrin-releasing peptide- and adrenocorticotrophic hormone-containing cells in the human lung. *Lab. Invest.* 48; 623–632.
  65. Tsutsumi, Y., Kawai, K., Hori, S. and Osamura, R. Y. (1991) Ultrastructural visualization of human papillomavirus DNA in verrucous and precancerous squamous lesions. *Acta Pathol. Jpn.* 41; 757–762.
  66. Tsutsumi, Y. (1994) Application of the immunoperoxidase method for histopathological diagnosis of infectious diseases. *Acta Histochem. Cytochem.* 27; 547–560.
  67. Tsutsumi, Y. (2000) Atlas of Infectious Disease Pathology. Bunkodo, Tokyo. <http://pathos223.com/atlas/index.htm> (in Japanese)
  68. Tsutsumi, Y. (2003) Pathology of Infectious Diseases. <http://pathos223.com/en>
  69. Tsutsumi, Y. and Hirasawa, Y. (2004) Special staining. I. *Byori-to-Rinsho* 22; 959–963 (in Japanese).
  70. Uchida, S., Shirotani, K. and Shinagawa, Y. (1961) Specimen preparation for electron microscopy from paraffin-embedded material. *J. Electron Microsc.* 10; 271–272 (in Japanese with English abstract).
  71. van den Bergh, W. M. A. and Dingemans, K. P. (1984) Rapid deparaffinization for electron microscopy. *Ultrastruct. Pathol.* 7; 55–57.
  72. Vardell, I. M., Lloyd, R. V., Wilson, B. S. and Polak, J. M. (1985) Ultrastructural localization of chromogranin: a potential marker for the electron microscopical recognition of endocrine cell secretory granules. *Histochem. J.* 17; 981–992.
  73. Wang, N.-S. and Minassian, H. (1987) The formaldehyde-fixed and paraffin-embedded tissues for diagnostic transmission electron microscopy: a retrospective and prospective study. *Hum. Pathol.* 18; 715–727.
  74. Watanabe, W., Kurumada, T., Shirai, T. and Tsutsumi, Y. (1995) Aberrant insulinoma of the duodenal bulb. *Pathol. Int.* 45; 895–900.
  75. Weidmann, J., Freund, M. and McGeever-Rubin, B. (1987) Comparative light and electron microscopy of paraffin-embedded tissue: an assessment of three methods. *J. Histochemol.* 10; 163–166.
  76. Widehn, S. and Kindblom, L.-G. (1988) A rapid and simple method for electron microscopy of paraffin-embedded tissue. *Ultrastruct. Pathol.* 12; 131–136.
  77. Yamamoto, I., Nakagawa, T. and Nakagawa, S. (1969) Comparative study of buffered, neutralized and unbuffered formalin with respect to preservation of ultrastructure. *J. Electron Microsc.* 18; 308–311 (in Japanese with English abstract).
  78. Yamamoto, I. and Takahashi, M. (1972) Electron microscopy of formalin-fixed biopsy and autopsy material. *Rinsho Byori* 20; 689–701 (in Japanese).
  79. Young, N. A., Naryshkin, S. and Katz, S. M. (2006) Diagnostic value of electron microscopy on paraffin-embedded cytologic material. *Diagn. Cytopathol.* 9; 282–290.